Hindawi
Shock and Vibration
Volume 2023, Article ID 9549121, 19 pages
https://doi.org/10.1155/2023/9549121

Research Article

Probabilistic Evaluation of Seismic Performance of Steel Buildings with Torsional Irregularities in Plan and Soft Story under Mainshock-Aftershock Sequence

Hamed Kouhestanian,[1] **Mohammad Hossein Razmkhah**,[2] **Jalil Shafaei**,[1] **Hossein Pahlavan**,[1] **and Mohammad Shamekhi Amiri**[1]

[1]*Departement of Civil Engineering, Shahrood University of Technology, Shahrood, Iran*
[2]*Departement of Civil Engineering, Semnan University, Semnan, Iran*

Correspondence should be addressed to Jalil Shafaei; jshafaei@shahroodut.ac.ir

Received 15 May 2023; Revised 2 July 2023; Accepted 6 July 2023; Published 12 July 2023

Academic Editor: Roberto Nascimbene

Due to the tectonic plate movement, numerous aftershocks may occur following an earthquake. There are several real mainshock-aftershock ground motion records in which the peak ground acceleration of aftershock is greater than that of the mainshock. Furthermore, irregularities such as soft story and torsional irregularity may change the structural behavior under the influence of earthquakes. This study investigates the fragility curves associated with the three-, five-, and eight-story models with steel moment-resisting frames under the main earthquake and mainshock-aftershock sequence to probabilistically evaluate the aftershock impacts on the steel structures with irregularities in the plan and height. The seismic fragility curves were calculated for four damage levels by selecting the relative displacement capacity at seismic performance levels of slight, moderate, extensive, and complete damage from the US HAZUS code. The analysis was done using structural reliability relationships and incremental dynamic analysis with the OpenSees software platform. The analytical results showed that the structures with soft-story and torsional irregularity were more vulnerable with an increasing number of stories. Also, aftershocks were found to have a more destructive effect on low-rise models. The probability of structural collapse in a given peak ground acceleration for a damaged state due to the mainshock-aftershock sequence is higher than that of the mainshock sequence.

1. Introduction

An earthquake refers to sudden slip on a fault and the resulting ground shaking and radiated seismic energy caused by volcanic and magmatic activities or other sudden stress changes in the Earth. Earthquakes are likely to occur worldwide and cause great life and financial losses. It is impossible to predict and prevent earthquakes. However, its casualties can be minimized by designing and constructing safe structures and detecting and improving unsafe buildings. It is not uncommon to observe aftershocks following a mainshock during an earthquake, where a big first shake on the 20th of May 2012 has been followed by a second big aftershock on the 29th of May [1]. The magnitude of an aftershock is usually less than the mainshock. Still, the former may have a higher PGA than the mainshock with an even longer duration and different energy content [2].

After the 2011 Great Tohoku earthquake in Japan, 588 aftershocks with M5.0 or greater were recorded, with 60 aftershocks being over M6.0 and three over M7.0. These strong aftershocks contributed to the collapse of many buildings that sustained damage from the mainshock, causing even more life losses. Li et al. investigated the collapse probability of mainshock-damaged steel buildings in the aftershocks. They indicated that aftershocks can cause severe damage to buildings and threaten life safety even when only minor damage is caused by the mainshock [3].

Also, the influence of the aftershock to mainshock PGA ratio on the structural vulnerability was investigated [4].

It has been found that the structural failure capacity can be significantly reduced when a high-intensity mainshock affects the structure. The likelihood of the structure collapse greatly increases even under a small aftershock after the mainshock. On the other hand, studying the behavior of structures in the past earthquakes has shown that order and symmetry in the structure's architectural plan, shape, and lateral force-resisting system arrangement strongly affect their seismic behavior. Observations have indicated that the structural asymmetry leads to increased damage during earthquakes (see Figure 1). In many constructed buildings, concerning several issues related to the parking provision and commercial and improper uses of masonry infills, there are sudden stiffness variations in the stories, which cause vulnerability to the earthquakes due to soft and even extreme soft stories. The present paper investigates the increasing structural damage in the presence of torsional irregularities in the plan and soft-story irregularities in the height. Moreover, the simultaneous impact of these irregularities under the influences of mainshock and mainshock-aftershock sequences is examined.

A probabilistic vulnerability assessment is warranted to examine the vulnerability of these structures and present improvement plans for the existing steel structures with a soft-story and torsional irregularity in the plan affected by the mainshock-aftershock sequences. The current research investigates the effects of an earthquake on the fragility curves. Steel structures are evaluated based on the construction methods in Iran and according to the Iranian regulations with the soft story and irregularity in the plan influenced by the mainshock-aftershock sequence.

Fragility curves were first employed to assess the vulnerability of the nuclear facilities since their smallest vulnerability to earthquakes is extremely dangerous. In this regard, these curves were plotted in 1980 for the nuclear power plants affected by various factors based on the peak ground acceleration (PGA) [5].

Razmkhah et al. investigated the fragility curve for the steel moment frame seismic system and indicated that the damage state of the structure due to soft story irregularity was decreased with increasing stories. On the other hand, the damage caused by torsional irregularity in plan was increased by increasing the structure's height [6].

Reza Salami et al. implemented a nonlinear finite element model for the inelastic buckling and low-cycle fatigue degradation of longitudinal reinforcement and simulated the multiple failure modes of RC columns under dynamic loading. They found that multiple excitations due to aftershocks can increase the damage of RC columns, and longitudinal reinforcements significantly affect the low-cycle fatigue. Furthermore, it was concluded that the rectangular column is more sensitive to accumulative damage due to cyclic fatigue [7].

Li et al. [3] examined the failure potential of damaged steel buildings by aftershocks as an essential part of the framework for integrating the seismic aftershock hazard into performance-based engineering (PBE). The four-story reinforced model was calibrated using available NEEShub data in this study. Three methods were used to create the fragility causing particular damage to the steel structures from the main earthquake to investigate the impact of the damage status due to the main earthquake on the structural failure capacity. The results suggested that the structure will probably fail even if the aftershocks are smaller than the main earthquake. Moreover, the effects of the main earthquake, fault type, and spectral shape of the aftershocks on the structural failure capacity have been evaluated.

Song et al. [8] estimated the damage caused by mainshock-aftershock sequences to the steel structures. They analyzed a typical four-story frame with one damage type. The main earthquake and aftershocks were simulated as homogeneous and nonhomogeneous Poisson processes, respectively, and the corresponding magnitude was determined using the Gutenberg–Richter relationship. Two earthquake levels of the design earthquake (DE) and maximum considered event (MCE) were expected to affect the building, and aftershocks were then applied to the structure after a period of inertia. The Monte Carlo simulation (MCS) and the Latin hypercube sampling (LHS) were used to investigate the uncertainty in the damage estimation. The results indicated that even if the aftershocks have little effect on the structural response, they might significantly impact the uncertainties in the damage status and cost estimates [9].

Pang and Wu investigated the influence of aftershocks on the reinforced concrete bridges, plotted the corresponding fragility curves via MCS, and concluded that the aftershocks increase the fragility of these bridges [10].

Using fragility curves and incremental dynamic analysis (IDA), Veismoradi et al. [11] investigated the different damage levels to the structures braced by the BRB system under mainshock-aftershock sequences. They concluded that the structures under mainshock-aftershock sequences experience displacements, being 1.5 times larger than those associated with a single earthquake.

Fattahi and Gholizadeh [12] studied the seismic performance of optimized steel moment frames (SMFs) within the framework of the performance-based design (PBD). The SMF design was first optimized and then analyzed by IDA in this study. Also, the fragility curves were plotted to evaluate the failure levels. Their findings illustrated that the design optimization might be cost-effective to the extent of complete damage [12].

Zhang and Burton qualitatively investigated the residual structural capacity of high-rise earthquake-damaged buildings through a pattern recognition approach [13]. They implicitly analyzed the history of nonlinear responses using aftershock and mainshock motions to create patterns with distinctive features of the engineering demand parameters (EDPs) in tall buildings. The residual structural capacity was evaluated based on the average spectrum intensity corresponding to the whole damage performance level. The predicted models were created using vector support to interpret EDP-based features for the residual structural capacity of the high-rise building, where satisfactory performance is observed by measuring the root mean square errors in the test dataset. In addition to post-seismic investigations and residual structural capacity assessment, the proposed framework could provide the optimal sensor placement and time-dependent limit state assessment in post-seismic environments.

Figure 1: Damage caused by soft-story irregularities in a past earthquake.

The current study investigates the effects of soft-story and torsional irregularities on the four damage levels of a steel structure with an intermediate moment-resisting frame affected by the earthquake and mainshock-aftershock sequence following HAZUS-MH MR-5 [14]. The effect of the first story's lateral stiffness reduction due to the soft-story and torsional irregularities is examined in the plan during an earthquake on the three-, five-, and eight-floor SMF models. This procedure was carried out by plotting the fragility curves for the four damage levels. The soft-story irregularity can occur due to various reasons, such as improper use of masonry infills, height increase, and removal of load transferring members to provide parking space. In this study, we focused on stiffness reduction and soft-story irregularity due to the increased height of the first story. Furthermore, torsional irregularities are due to the asymmetric use of the lateral resisting system, a wide span in the diaphragm, plan asymmetry, excessive gravity concentration on one side of the plan, etc. Here, the irregularities due to the asymmetry of the lateral resisting system were studied.

In the structural design standards, the effect of aftershocks on the structure's seismic performance is not recommended. Also, previous studies have not investigated the effect of the soft-story and torsional irregularities on the plan simultaneously affected by main shock and aftershock. Many buildings in seismic areas have these two irregularities at the same time, and the results of this research can pave the way for design engineers in this field. In this research, OpenSees software has been used for nonlinear dynamic analysis. This software is used because of its high capability in nonlinear analysis on a large scale. The fragility curves from selection of earthquake hazards to implementing framework in the model are presented in Figure 2.

2. Explanation of the Models Used in the Present Study

The 3-D models used in the present study have three, five, and eight stories, with the following characteristics: (a) a regular structure in height and plan, (b) a regular structure in plan with soft-story irregularity in the first story (buildings are classified as soft story if a level is less than 70% as stiff as the floor above it or less than 80% as stiff as the average stiffness of the three floors above it, according to the International Building Code (IBC) definition), and (c) structure with simultaneous effects of soft-story and torsional irregularities on plan by moving the axis of the beams and columns (buildings have torsional irregularity in plan if the maximum relative displacement of one end of a building in a story divided by average displacement of the two ends in the same story is more than 1.2, according to the IBC definition), whose lateral force-resisting system is an intermediate SMF (Figure 3(b)). The building is designed according to the associated regulations in Iran. The model specifications are given as follows:

(i) The structure is designed in an area of high relative risk.

(ii) The soil of the construction site is assumed to be of type III.

(iii) The height of the first story for regular structures in height and structures with soft-story irregularity is 2.8 and 3.8 m, respectively, and that of other stories is considered to be 3.2 m (described in Section 4).

(iv) The yield stress of the steel used for the beams and columns is equal to 240 MPa.

(v) The ultimate stress of the steel used for the beams and columns is 370 MPa.

Based on the unit force to the first-story diaphragm and its displacement in ETABS (ETABS Version 18.0.2) software, the first story stiffness was examined using equation $F = K\Delta$. Then, the second story's stiffness was calculated. If the first to second story stiffness ratio is between 60 and 70%, the structure has a soft-story irregularity.

In addition to ETABS software, the lateral stiffness of each story can be calculated using equation $K = 12EI/L^3$. Estimation of the stiffness of the models demonstrated that in structures with the first story of 3.8 m high, the stiffness is 0.61 times more than that of the second story, indicating a soft-story irregularity.

2.1. Overview of the OpenSees Software Framework. OpenSees is an object-oriented, open-source framework developed to simulate the response of structural systems subjected to earthquakes by researchers at the Pacific Earthquake Engineering Research (PEER) Center. OpenSees (OpenSees Version 2.0.5) was chosen for dynamic and static

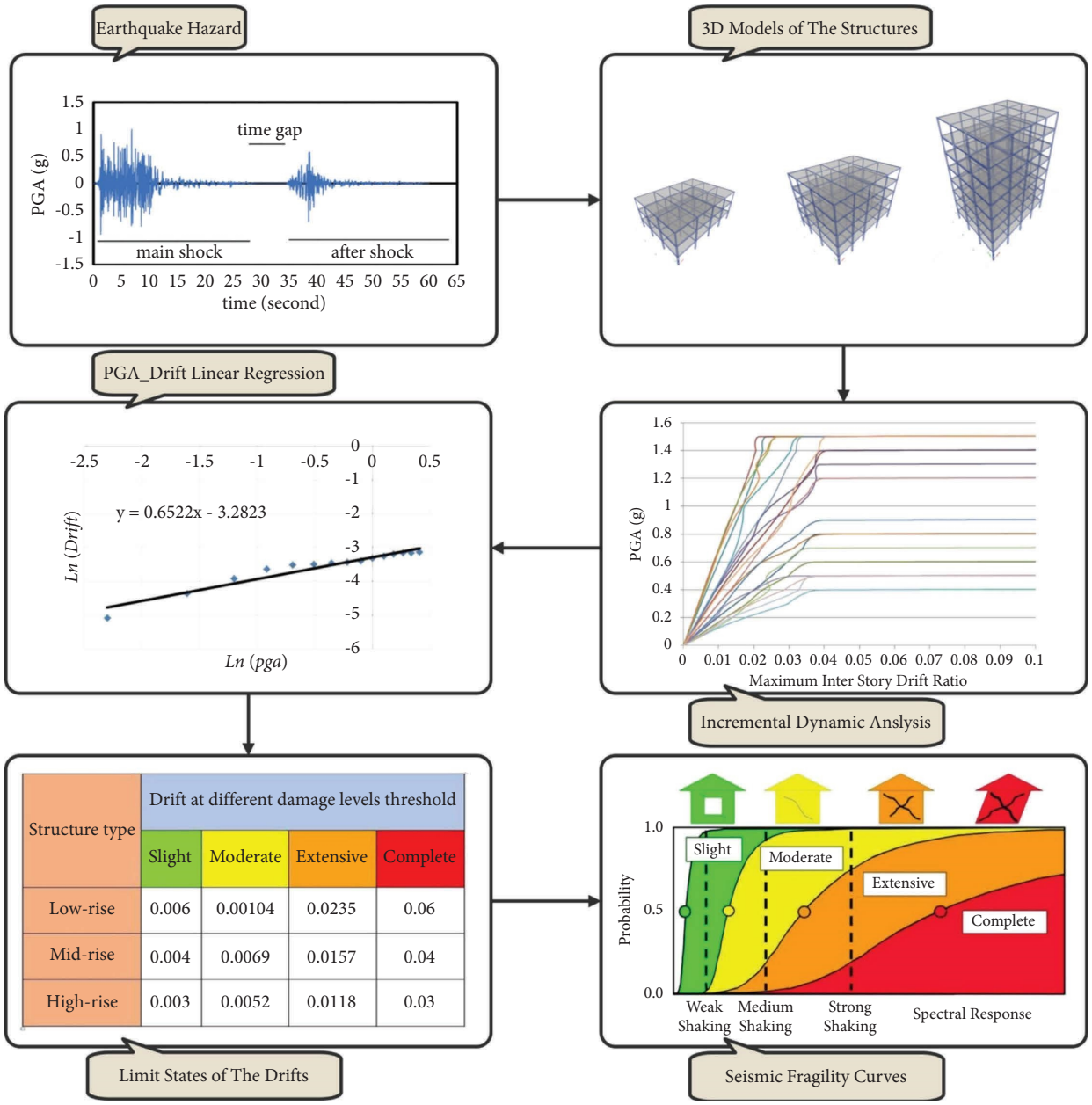

Figure 2: Implemented framework of the probabilistic seismic vulnerability assessment.

analysis of selected frame due to its relative ease with the new joint element formulation, nonlinear beam-column element formulations, and global solution algorithms. OpenSees involves several models for describing material (steel and concrete) behavior. The member stiffness and forces are obtained by numerically integrating the stiffness and forces of sections along the member length. The section deformation is used to obtain the strain in each fiber, based on the plane section assumption. The fiber stress and stiffness are updated according to the corresponding material models, followed by upgrading the section force and the corresponding stiffness.

2.2. Validating the Proposed Numerical Model with the Experimental Results. In order to validate the simulation results, the OpenSees software outputs are compared with the experimental results due to an actual sample. To ensure the model's validity, the structure period modeled in OpenSees is compared with that of ETABS software and the empirical relationships listed in Standard 2800 [15]. The results are presented in Table 1.

Given the close agreement between the periods extracted from the OpenSees software and those of the experimental approach, it is concluded that the OpenSees modeling has estimated the stiffness with acceptable accuracy. Then, the

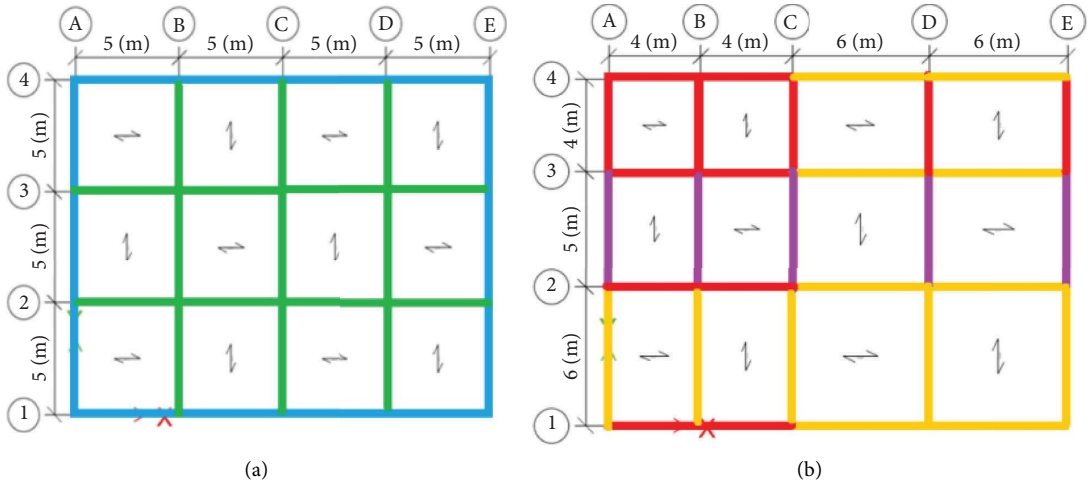

(a) (b)

Figure 3: The typical story plan of the Model: (a) structure with a regular plan; (b) structure with an irregular plan.

Table 1: Different periods of the studied structures.

Number of stories	Structure periods of the regular structures in plan and height		
	ETABS	OpenSees	Empirical relationships
Three-story	0.56	0.49	0.42
Five-story	0.76	0.68	0.63
Eight-story	1.20	1.13	0.9
Periods of the structures with a soft story			
Three-story	0.61	0.52	0.46
Five-story	0.81	0.73	0.66
Eight-story	1.21	1.13	0.93
Periods of the structures with the soft-story and torsional irregularities			
Three-story	0.64	0.54	0.46
Five-story	0.84	0.75	0.66
Eight-story	1.22	1.15	0.93

experimental model results are compared with those obtained via OpenSees software to validate the materials and elements.

Figure 4 shows the model of a four-story, two-span frame with a special moment-resisting frame (SMRF) system used in an administrative in Los Angeles, California. The soil of the construction site is of type D, with a column axis-to-axis length of 9100 mm and a first-story height of 4600 mm. Other stories are 3700 mm high. The structure design was based on IBC2003 [17], and the gravity and lateral loads were calculated and applied to the structure using ASCE-7 2013 [18] and AISC2005 [19], respectively.

The beam element sections used for the first, second, third, and fourth stories are considered W27X102 and W21X93, respectively. Moreover, the first, second, third, and fourth story columns are W24X131 and W24X76, respectively. The A992 Grade 50 steel was for all structural steel components. The seismically effective weight was 4.6 kN (1050 kips) for each of the first three floors and 5.3 kN (1200 kips) for the roof. The model frames were built and tested via the NEES facility at the State University of New York at Buffalo. The Canoga Park record Station of the Northridge earthquake in 1994 with different grand motion accelerations was entered, and the maximum drift of the roof was calculated. The details associated with the model and tests can be found in Lignos et al. [16]. The results of the two approaches are compared by plotting the force-displacement curve corresponding to the experimental and simulated models in Figure 5.

2.2.1. Material Behavior Model. This study used uniaxial materials with uniaxialMaterial command to define the steel materials. Steel02 command is used for steel materials, including the isotropic hardening, and considers the loss of resistance and tearing conditions [20].

Fiber sections were used to define the beam and column sections in OpenSees. Via characteristics of the fiber sections, different material properties can be applied in each section of the element length with the help of these sections. The fiber model for an I-shaped steel section is depicted in Figure 6.

Since the analysis in this study was nonlinear, the nonlinear BeamColumn command was used to define its elements. The nonlinear elements can be modeled by using this command. This command distributes the inelastic effects throughout the element. After reviewing and selecting the material behavioral model in OpenSees, this software modeled the experimental sample with the same gravity, lateral loading, and roof drift due to PGA extraction. A comparison of the displacements associated with the experimental and simulated models is shown in Figure 5.

As shown in Figure 5, the simulation and experimental results are in close agreement.

2.3. Earthquake Accelerogram Selection. The earthquake record-setting is one of the most important steps in the nonlinear dynamic analysis as IDA results depend on record type. Records must be selected in such a way to encompass all behavioral modes of the structure.

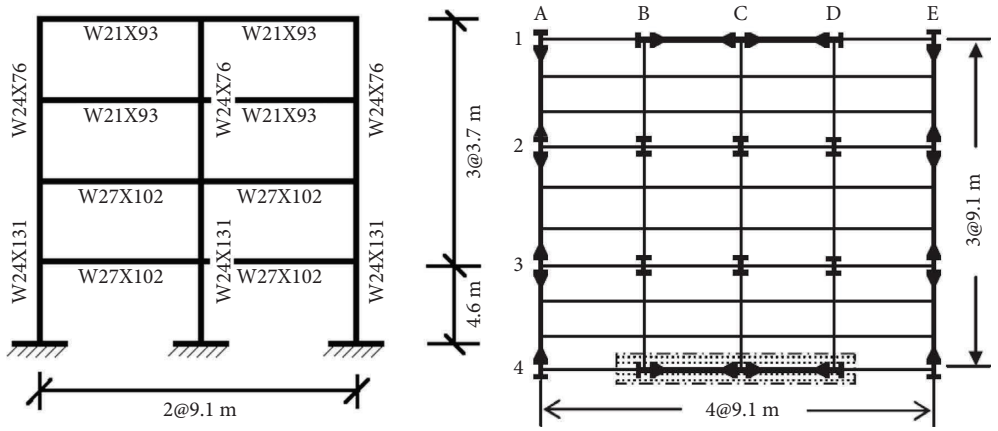

Figure 4: Details of the 2-D frame dimensions for validation [16].

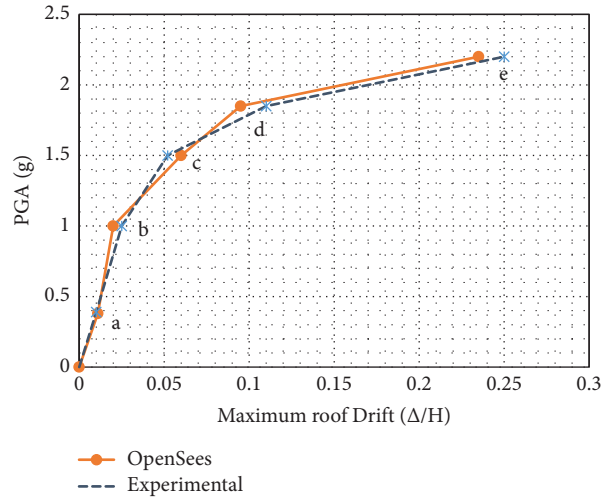

Figure 5: Comparison of the experimental IDA curve with OpenSees software simulation.

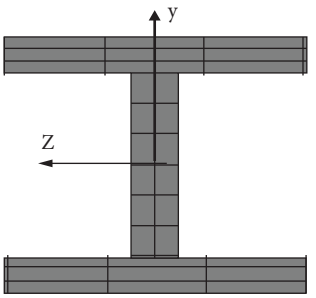

Figure 6: Fiber model for a steel I-shaped cross section [23].

In this study, 20 earthquake records were selected from the Peer site according to the site's soil type and Li et al.'s criteria [3]:

(i) According to the site's soil type, the soil should have a shear velocity of 175–375 m/s.

(ii) Aftershock magnitudes should be at least 0.5 g.

(iii) PGA should be greater than 0.4 g.

Table 2 presents the selected records.

2.4. Mainshock-Aftershock Integration. There is a time gap between the main earthquake and aftershock. During this period, the model under the main earthquake accelerogram

Table 2: Selected earthquake records.

Record number	Record name	Station name	Soil type	Earthquake magnitude (Richter)	PGA (g)
1	Chalfant Valley	Zack Brothers Ranch	III	6.19	0.447
2	Coalinga	Oil City	III	5.77	0.398
3	Northridge	Sun Valley-Roscoe Blvd	III	6.69	0.604
4	Imperial Valley	El Centro Array #11	III	6.53	0.37
5	Coalinga	14Th & Elm (Old CHP)	III	5.77	0.84
6	Imperial Valley	Bonds Corner	III	6.53	0.776
7	Mammoth Lakes	Convict Creek	III	6.06	0.444
8	Mammoth Lakes	Fish & Game (FIS)	III	5.94	0.376
9	Mammoth Lakes	Mammoth Lakes H. S	III	5.69	0.44
10	Managua-Nicaragua	Managua-Esso	III	6.24	0.371
11	Northridge	Northridge-17645 Saticoy St	III	6.69	0.459
12	Northridge	Canoga Park-Topanga Can	III	6.69	0.392
13	Northridge	Jensen Filter Plant Administrative Building	III	6.69	0.617
14	Northridge	La-Sepulveda Va Hospital	III	6.69	0.93
15	Northridge	Newhall-Fire Sta	III	6.69	0.59
16	Northridge	Rinaldi Receiving Sta	III	6.69	0.87
17	Imperial Valley	El Centro array #4	III	6.53	0.48
18	Imperial Valley	El Centro Array #5	III	6.53	0.53
19	Imperial Valley	El Centro Array #7	III	6.53	0.57
20	Imperial Valley	El Centro Array #8	III	6.53	0.61

rests until vibration cessation is reached due to damping and nonmaintenance on the structure. Therefore, in order to simulate this in the real world, the models are first subjected to the earthquake accelerogram and then kept in the stillness position for 4 s. Thus, the permanent displacement due to the earthquake could only remain, and the main earthquake vibrations could stop due to the damping (see Figure 7). The structural model is then subjected to the aftershock accelerogram. It is worth mentioning that the time required for vibration attenuation depends on the regularity or irregularity type of the structure [21].

In this study, all main earthquake accelerograms were scaled to 1 g to plot the fragility curves and compare damage to the structures. In the mainshock-aftershock sequence mode, a new accelerogram is created by integrating the main earthquake, stillness, and aftershock, and all new accelerogram pulses increase in proportion by being scaled to 1 g. An example of the Mammoth Lakes-Convict Creek scaled mainshock-aftershock integration is shown in Figure 8.

3. Results and Discussion

The following results were obtained using the IDA method and the fragility curves in terms of earthquake intensity and structure response.

3.1. Hysteresis Curve. In order to evaluate the performance of the model and sections made in OpenSees software, the moment-curvature hysteresis curve is investigated. The hysteresis curves associated with the first story beam specified in Figure 9 under the Chalfant Valley earthquake at Zack Brothers Ranch station and scaled earthquake to 1g are shown in Figure 8.

The hysteresis curves associated with the first story column along the C-2 axis in Figure 9 under the Chalfant Valley earthquake at Zack Brothers Ranch station and scaled earthquake to 1 g are plotted in Figure 10.

Examining the hysteresis curves revealed that the beam and column elements had entered the nonlinear zone, indicating the ability of the analytical model to estimate the nonlinear response of the structural models.

3.2. Base Shear Comparison of the Studied Models. The base shear curve in terms of the roof displacement is one of the important curves in the seismic behavior of the structures, indicating how the structural stiffness, resistance, and degree change. Figure 11 plots the base shear curve regarding the roof displacement in three-story structures affected by the single earthquake and mainshock-aftershock sequences. Comparing the effects of torsional and soft-story irregularities on the base shear-roof displacement curve in structures with torsional irregularity shows that the base shear rate under the same displacement is increased by 7% due to the main earthquake. However, it increases by 3% under the effect of the mainshock-aftershock sequence. Besides, the base shear decreases by 12% when the structure is subjected to the effect of the mainshock-aftershock sequence.

3.3. Comparison of the Roof Displacement during the Earthquake. To compare the displacement of the examined structures during the earthquake, they were subjected to the Chalfant Valley earthquake record at the Zack Brothers Ranch station. Finally, permanent displacement can be observed in these structures (see Figures 12 and 13).

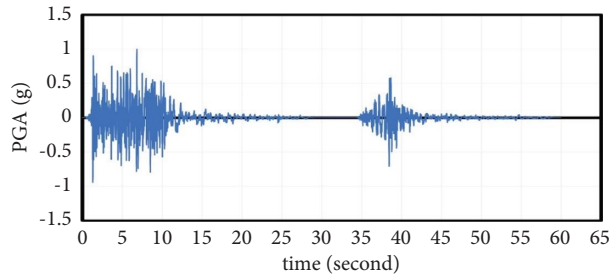

Figure 7: Scaled Mammoth Lakes-Convict Creek earthquake accelerogram.

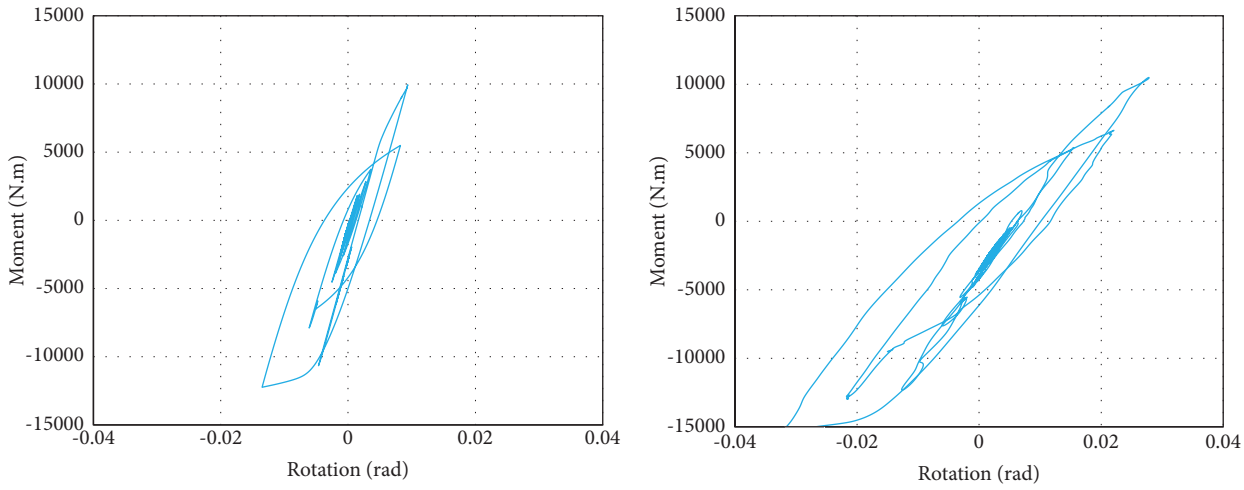

Figure 8: Beam moment-curvature cyclic curve in a five-story structure with (a) soft-story irregularity and (b) soft-story and torsional irregularity.

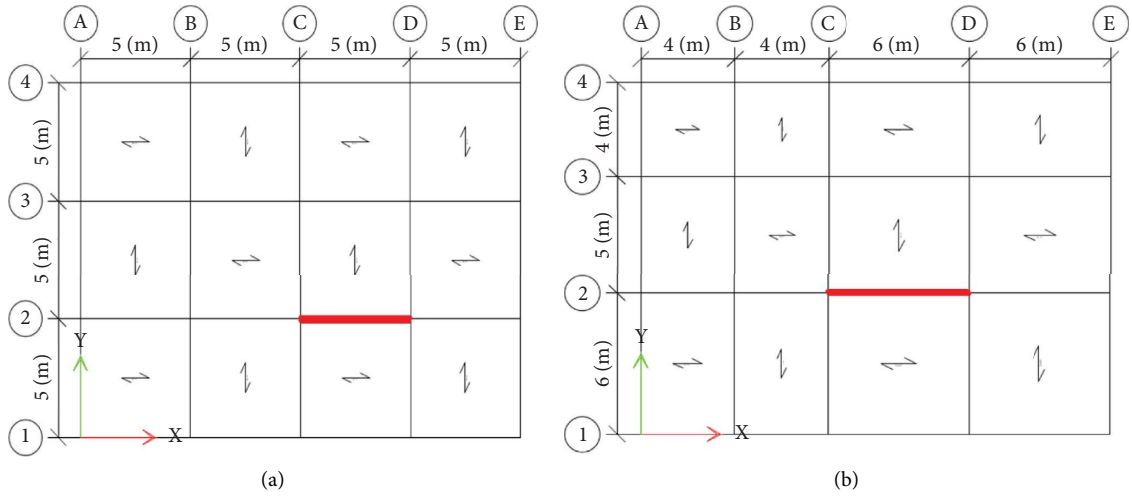

Figure 9: Selected beam for plotting the hysteresis curve structure with (a) a regular plan and (b) an irregular plan.

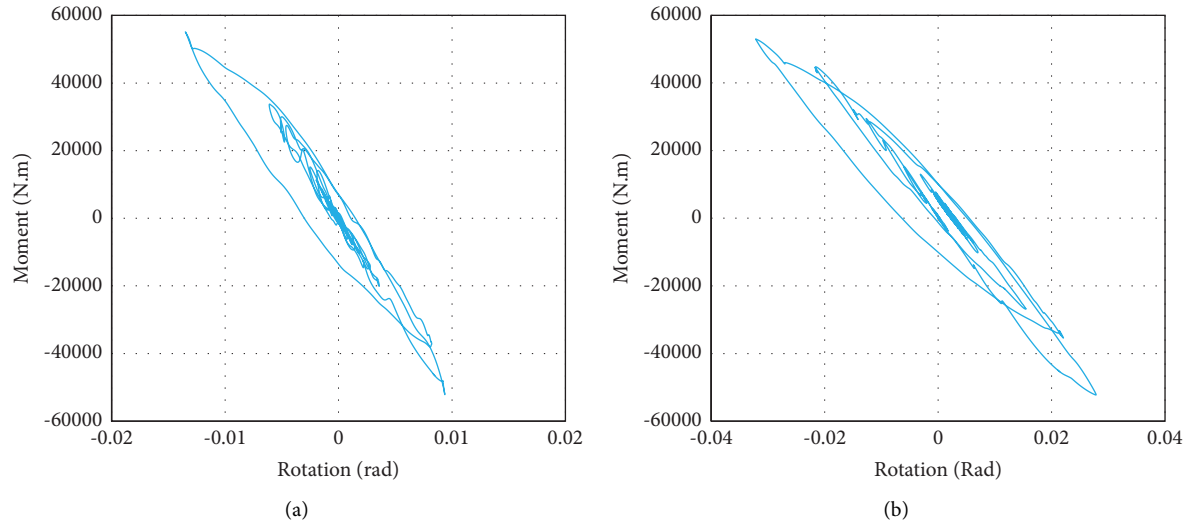

Figure 10: Column moment-curvature cyclic curve in a five-story structure with (a) soft-story irregularity and (b) soft-story and torsional irregularity.

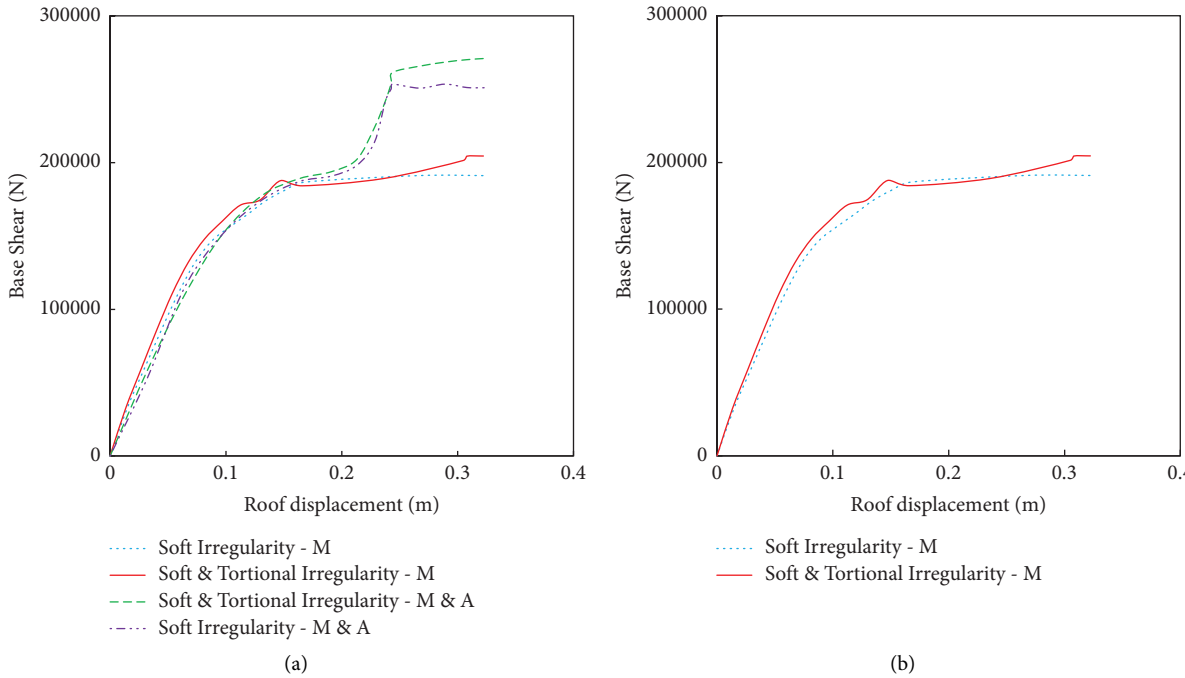

Figure 11: Continued.

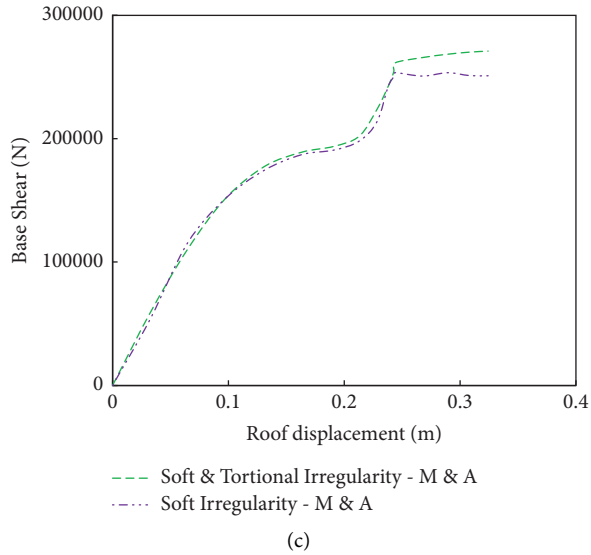

(c)

Figure 11: Displacement-base shear diagram of the three-story models under (a) the effect of the main earthquake and mainshock-aftershock sequence with soft irregularity and torsional irregularity; (b) the mainshock; and (c) the main earthquake-aftershock sequence.

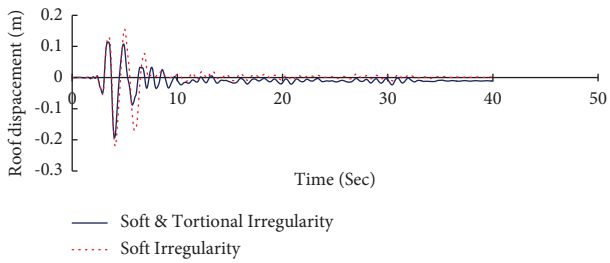

Figure 12: Roof displacement variation during the earthquake in two three-story structures with the soft-story irregularity and simultaneous effect of the soft-story and torsional irregularities under the effect of the mainshock.

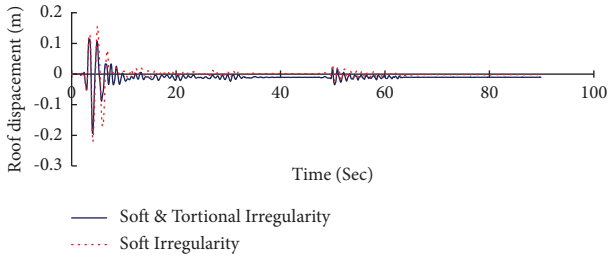

Figure 13: Roof displacement variation during the earthquake in two three-story structures with the soft-story irregularity and simultaneous effects of the soft-story and torsional irregularities under the effect of the mainshock-aftershock sequence.

The figures reveal that in the three-story structures, the permanent displacement in structures with simultaneous effects of the soft-story and torsional irregularities is always greater than the one with soft story. Moreover, the displacement amplitude in structures with soft-story irregularity is greater than those with both aforementioned irregularities.

3.4. Definition of the Damage Levels. The damage levels in accordance with the HAZUS-MH MR-5 instruction include slight, moderate, extensive, and complete damage. Table 3 lists the maximum displacement amounts corresponding to these damage levels.

According to this instruction, the best point representing the demand at the damage threshold performance level occurs when the softening reaches the total dynamic instability. Another damage criterion is the maximum drift or relative displacement between the stories. The maximum drift for short, medium, and tall structures is given in Table 3 based on HAZUS-MH MR-5.

3.5. IDA Curves. IDA involves multiple nonlinear dynamic analyses of a structural model under a suite of ground motion records, and each is scaled to several seismic intensity levels. The scaling levels are appropriately selected to force the structure on the entire range of behavior, from elastic to inelastic, and finally to global dynamic instability, where the structure essentially experiences collapse. IDA analysis identifies the structure capacity, damage probability, and percentage of exceeding a certain damage level, all of which make this analysis superior to the pushover one. Introducing materials with nonlinear behavior can be pointed out as another feature of the IDA analysis [22].

In the IDA analysis of the present study, the PGA introduced to the structure was divided into steps of 0.1 g. Then, the IDA curves were plotted using the structural analysis at each step. The IDA curves for the three-, five-, and eight-story models are plotted under the effects of the main earthquake and mainshock-aftershock sequences with 20 accelerograms (see Figures 14–16).

In addition, incremental nonlinear dynamic analysis was used to consider the uncertainties of earthquake records, including frequency content. This uncertainty is one of the most important aspects of evaluating seismic performance of

Table 3: Drift values at different damage levels according to HAZUS-MH MR-5 [13].

Structure type	Drift at different damage level threshold			
	Slight	Moderate	Extensive	Complete
Low-rise	0.006	0.00104	0.0235	0.06
Mid-rise	0.004	0.0069	0.0157	0.04
High-rise	0.003	0.0052	0.0118	0.03

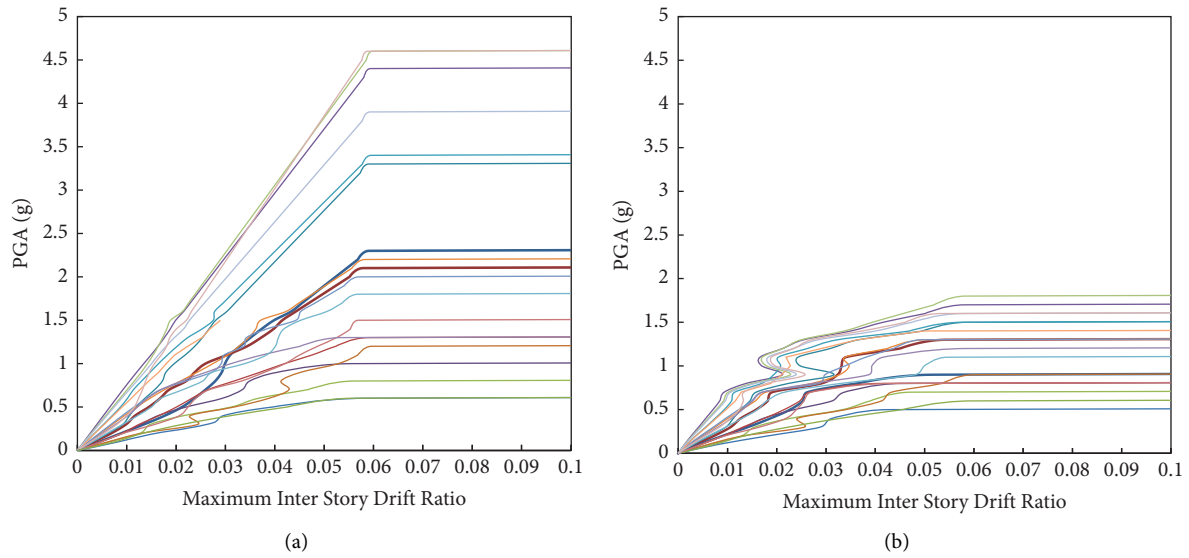

Figure 14: IDA diagram of a three-story structure with soft-story irregularity under the effect of (a) mainshock and (b) mainshock-aftershock sequence.

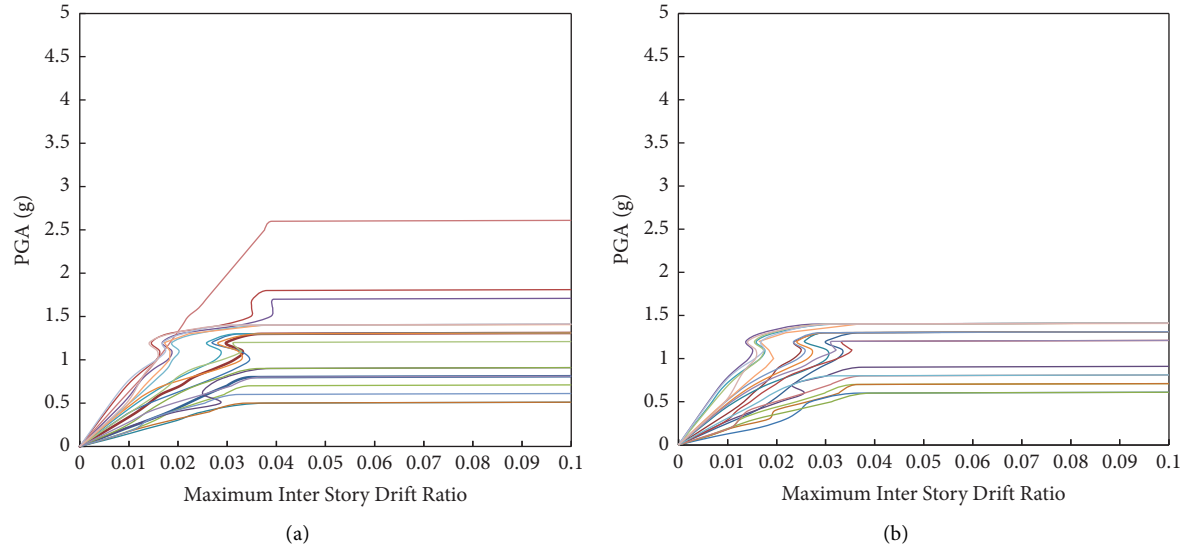

Figure 15: IDA diagram of a five-story structure with soft-story irregularity under the effect of (a) mainshock and (b) mainshock-aftershock sequence.

structures. This method can also consider the stiffness and resistance deterioration in each cycle. In contrast, the pushover analysis cannot consider these items due to its noncyclic and monotonic nature.

The IDA analysis diagrams show that structures have experienced severe hardening under accelerograms in most cases, indicating that the displacement has hardly occurred.

3.6. Generating and Plotting the Fragility Curve. The fragility curves help assess the probability of damage to the structures. An important point in producing a fragility curve is the difference between the characteristics of structures in each country. Therefore, structure specifications must be taken into account in the structural analysis. A probability distribution for the engineering demand parameters

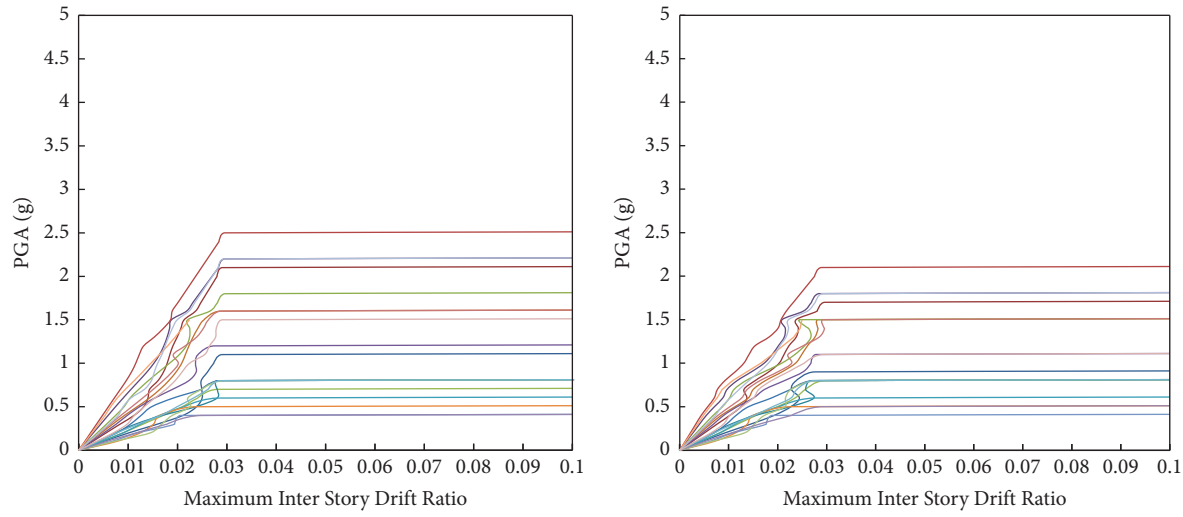

Figure 16: IDA diagram of an eight-story structure with soft-story irregularity under the effect of (a) mainshock and (b) mainshock-aftershock sequence.

obtained from the IDA analysis is used to generate the fragility curve. In this study, the log-normal distribution was employed.

Each structure was analyzed under 20 earthquake records from 0.1 to 1.5 g, and then the probability of structural failure was investigated using OpenSees software.

When the structural capacity and seismic demand are two parameters that follow the normal distribution, the resulting combined performance has a normal logarithmic distribution with the aid of the central limit theorem. Thus, the fragility curves can be obtained according to the following relation.

$$P(D > C \mid IM) = \Phi\left(\frac{\ln(S_d) - \ln(S_C)}{\beta_{sd}}\right). \quad (1)$$

In the above equation, P is the probability of exceeding the demand (D) from the capacity of the structure (C) which is in terms of maximum inter-story displacement, β_{sd} is the standard deviation of log-normal, S_C stands for the average permissible limit state, and S_d defines the mean seismic demand.

Figure 17 shows the fragility curves associated with the four damage modes of a three-story model structure with soft-story irregularity. In addition, simultaneous effects of soft-story and torsional irregularities under the impacts of a single earthquake and mainshock-aftershock sequences records are depicted in Figure 17.

Figure 18 illustrates the fragility curves associated with the four damage modes of a five-story model structure with soft-story irregularity. Simultaneous effects of soft-story and torsional irregularities under the impacts of a single earthquake and mainshock-aftershock sequences records are depicted in Figure 18.

Figure 19 depicts the fragility curves associated with the four damage modes of an eight-story model structure with soft-story irregularity. The figure shows simultaneous effects of both soft-story and torsional irregularities under the impacts of a single earthquake and mainshock-aftershock sequences records.

3.6.1. Comparing the Structural Fragility Curves. This section investigates the fragility curves of three-, five-, and eight-story structures.

3.6.2. Comparing the Fragility Curves Corresponding to the Three-Story Model. The fragility curves for the three-, five-, and eight-story regular structures were first generated. Then, those with soft-story irregularity and simultaneous effects of both soft-story and torsional irregularities under the effects of earthquake and mainshock-aftershock sequence were compared separately.

Comparison of the slight damage level in the three-story model (Figure 20(a)) shows that the damage levels are nearly the same for the structure with soft-story irregularity and simultaneous effects of both soft-story and torsional irregularities affected by a single earthquake and mainshock-aftershock sequences. However, at the moderate damage level, the mainshock-aftershock sequence reduced the Earth's gravitational acceleration by 10% to achieve some level of damage in comparison with the case when the structure is only affected by a single earthquake. Also, at the extensive damage level, the damage level of the structure with soft-story irregularity is the same as that of the structure with simultaneous soft-story and torsional irregularities. In addition, the mainshock-aftershock sequence has led to the gravitational acceleration reduction by 23% compared to the structure analyzed under the effect of a single earthquake. Similarly, at the complete damage level, the damage rate in the structure with soft-story irregularity is identical to that of the structure with simultaneous soft-story and torsional irregularities. However, compared to the structural analysis

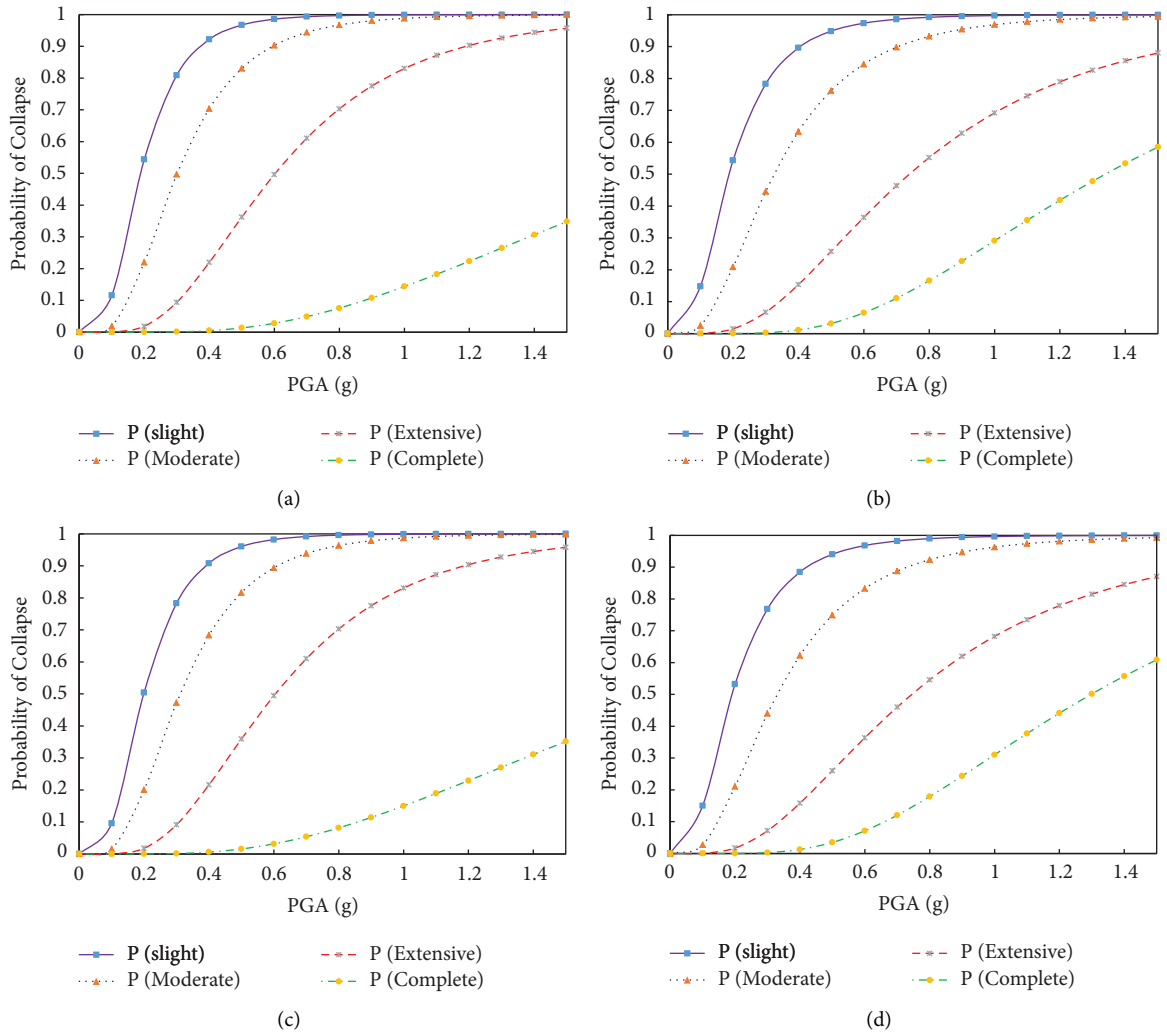

Figure 17: Fragility curve of a three-story structure with (a) soft-story irregularity affected by a single earthquake; (b) soft-story irregularity affected by the mainshock-aftershock sequence; (c) both soft-story and torsional irregularities affected by a single earthquake; and (d) both soft-story and torsional irregularities affected by the mainshock-aftershock sequence.

impacted by a single earthquake at a 30% damage level, the mainshock-aftershock sequence reduced Earth's gravitational acceleration by 37 and 40% in the structures with soft-story and simultaneous soft-story and torsional irregularities, respectively.

Comparing the three-story models with soft-story irregularity alone and simultaneous soft-story and torsional irregularities subjected to the mainshock and mainshock-aftershock sequences, we found that a soft story causes significant damage under aftershock. In contrast, that of torsional irregularity has no significant effect.

3.6.3. Comparing the Fragility Curves Corresponding to the Five-Story Model. This section compares the fragility curves associated with four slight, moderate, extensive, and complete damage levels for the five-story models affected by a single earthquake and mainshock-aftershock sequence records.

Comparing the slight damage level in the five-story model (see Figure 21) shows that this level is almost the same when the structure with soft-story irregularity and simultaneous soft-story and torsional irregularities is affected by a single earthquake and mainshock-aftershock sequences. At the moderate damage level, the effect of the mainshock-aftershock sequence is observable, which reduces the Earth's gravitational acceleration by 12% to achieve some level of damage compared with the case when the structure is only affected by a single earthquake. At the extensive damage level, it is observed that in structures with simultaneous soft-story and torsional irregularities compared to structures with soft-story irregularities, Earth's gravity acceleration reduces by 5% at a 50% probability of extensive damage.

At the extensive damage level, aftershocks have reduced the Earth's gravitational acceleration by 7 and 8.5% at a 50% probability of the corresponding damage, compared to the structures with soft story and simultaneous soft-story and

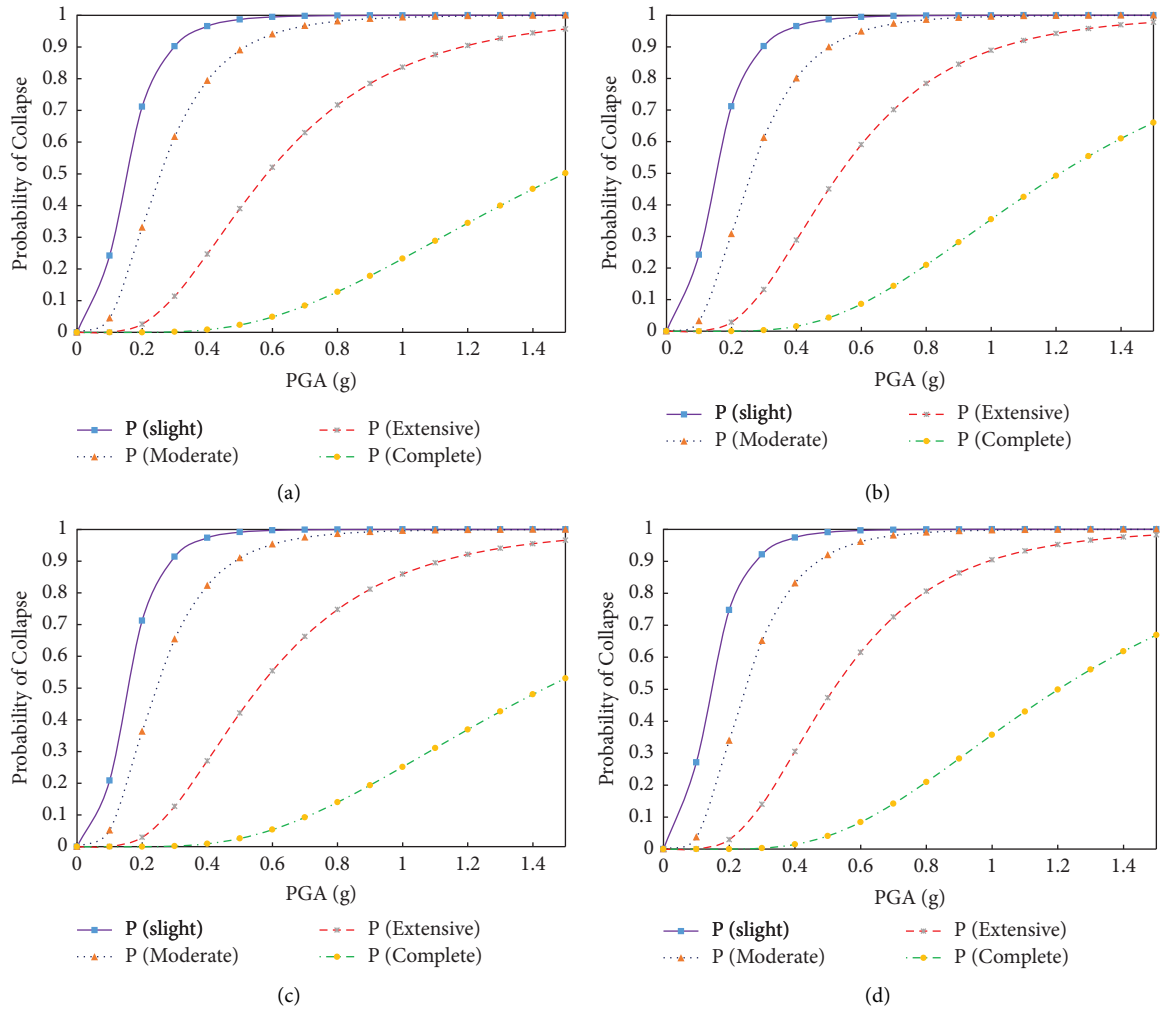

Figure 18: Fragility curve of a five-story structure with (a) soft-story irregularity affected by a single earthquake; (b) soft-story irregularity affected by the mainshock-aftershock sequence; (c) both soft-story and torsional irregularities affected by a single earthquake; and (d) both soft-story and torsional irregularities affected by the mainshock-aftershock sequence.

torsional irregularities subjected only to a main shock, respectively.

The complete failure diagram shows that at 50% probability of the corresponding damage level, the gravitational acceleration in structures with simultaneous soft-story and torsional irregularities is reduced by 6% compared to those with soft-story ones. Also, the mainshock-aftershock sequence effect reduces the Earth's gravitational acceleration by 17 and 20%, compared to the structures with soft-story and simultaneous soft-story and torsional irregularities affected by a single earthquake, respectively.

Comparing the five-story models with soft-story irregularity alone and simultaneous soft-story and torsional irregularities in the mainshock and mainshock-aftershock sequences indicated that the aftershock causes significant damage in these structures. In contrast, soft-story and torsional irregularities had no significant effect.

3.6.4. Comparing the Fragility Curves Corresponding to the Eight-Story Model. The fragility curves for three- and five-story models affected by a single earthquake and the mainshock-aftershock sequence were plotted and compared. Finally, similar curves were plotted for the four damage levels in the eight-story models.

Comparing the slight damage level in the eight-story model (see Figure 22) illustrates that the aftershock reduces the gravitational acceleration by 27 and 22% in structures with soft-story and simultaneous soft-story and torsional irregularities, respectively. However, at the moderate damage level, the aftershock decreased the gravitational acceleration by 10% in the structures with both irregularities compared to the cases affected by a single earthquake.

At the extensive damage level, the effect of the mainshock-aftershock sequence reduces the Earth's gravitational acceleration by 5 and 6% in structures with soft-story and

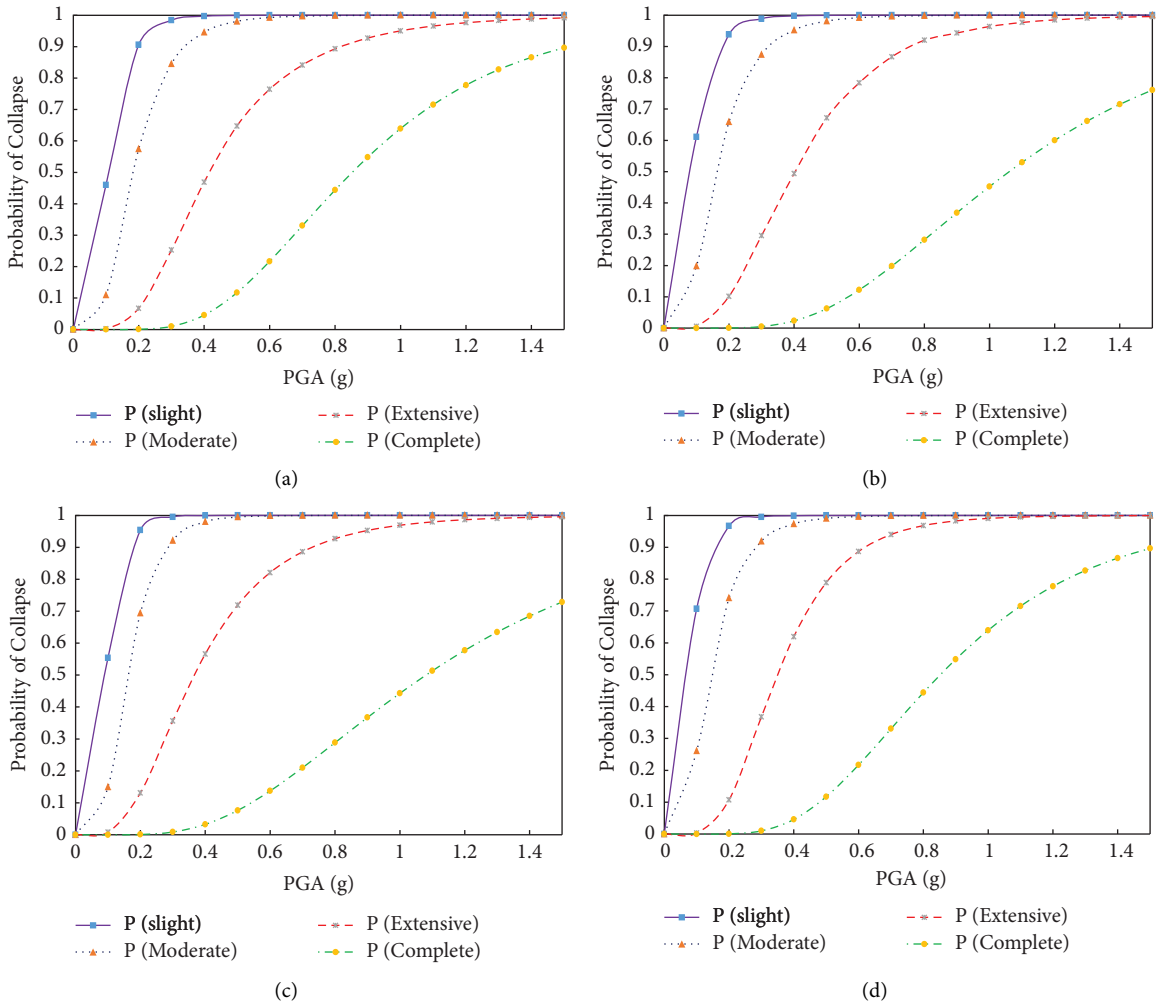

Figure 19: Fragility curve of an eight-story structure with (a) soft-story irregularity affected by a single earthquake; (b) soft-story irregularity affected by the mainshock-aftershock sequence; (c) both soft-story and torsional irregularities affected by a single earthquake; and (d) both soft-story and torsional irregularities affected by the mainshock-aftershock sequence.

simultaneous soft-story and torsional irregularities, respectively. In addition, at the complete damage level, the aftershock reduces the gravitational acceleration by 21 and 9% in the structures with simultaneous soft-story and torsional and soft-story irregularities, respectively. Also, at the damage level of 50%, the simultaneous effects of soft-story and torsional irregularities cause a 7% reduction in the gravitational acceleration compared to the structures with soft-story one.

Comparing the eight-story models with soft-story irregularity alone and simultaneous soft-story and torsional irregularities under the mainshock and mainshock-aftershock sequence illustrated that the torsional irregularity causes significant damage in these structures. However, the aftershock and soft-story irregularity had no significant effects.

3.6.5. Comparing the Structure Fragility Curves Corresponding to the Three-, Five-, and Eight-Story Models. The three-, five-, and eight-story steel structures with soft-story and simultaneous soft-story and torsional irregularities under the effect of a single earthquake and mainshock-aftershock sequence were investigated in the present study. The results indicated that a height difference does not affect slight and moderate damage levels, but its effect is significant at extensive and complete ones. Also, as the number of stories increases, the effect of soft story decreases for the four damage levels. The numerical results of the height increase effects in the three-, five-, and eight-story structures are as follows.

In the low-rise structures, the effect of height increase was greater and decreased with the increasing number of stories. Hence, in these structures, the height increase caused an increase of 5, 8, 9, and 4% in the slight, moderate, extensive, and complete damage levels, respectively. These increase rates were 3, 4, 5, and 3% in mid-rise structures. However, the height increment in high-rise structures only increased the extensive and complete damage levels by 2 and 3%, respectively.

In the low-rise structures, the effect of the aftershock was greater and decreased with the increasing number of stories. Therefore, the aftershock increased 5, 10, 23, and 37% in

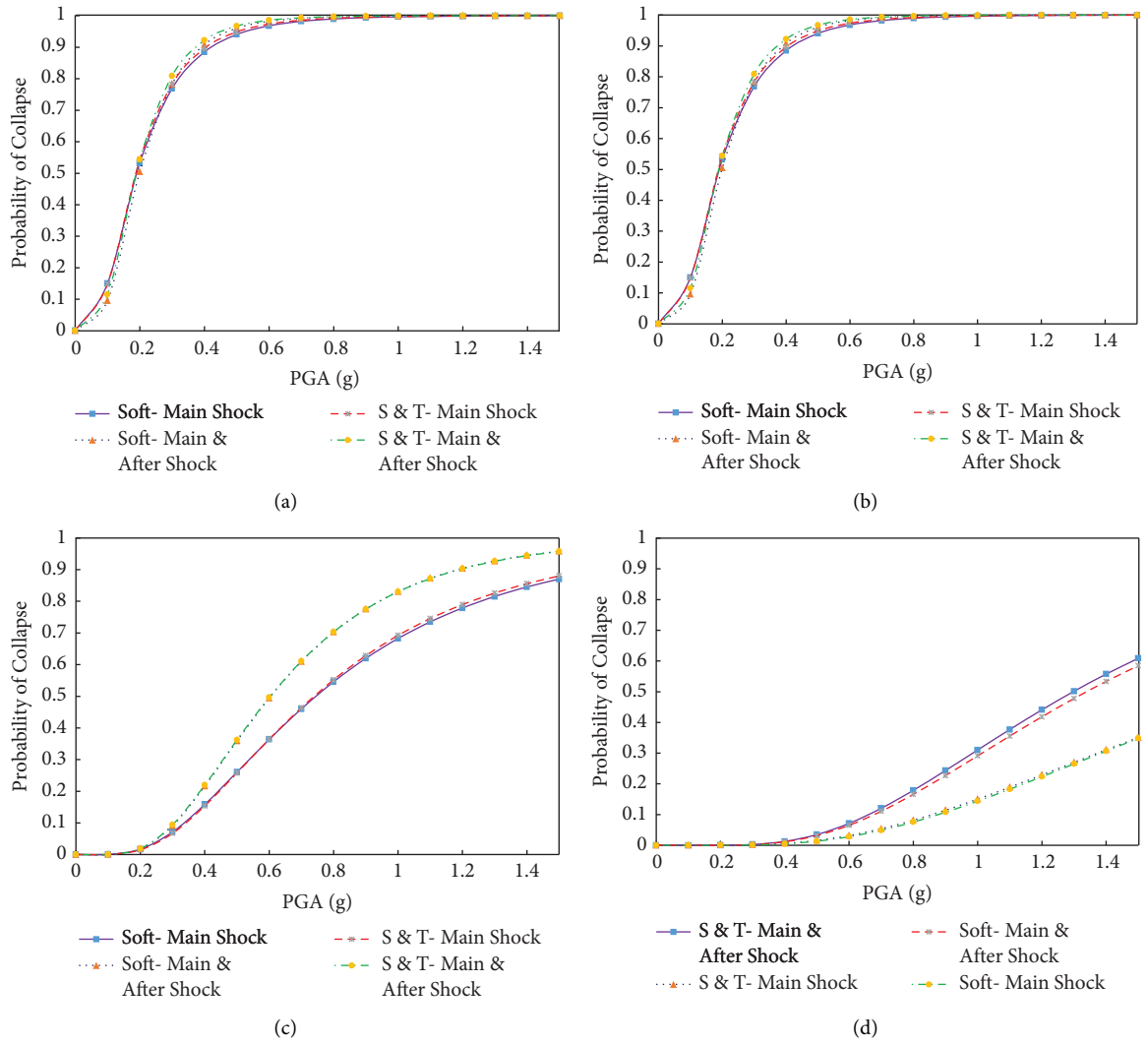

Figure 20: Fragility curve of a three-story structure for (a) slight damage level; (b) moderate damage level; (c) extensive damage level; and (d) complete damage level.

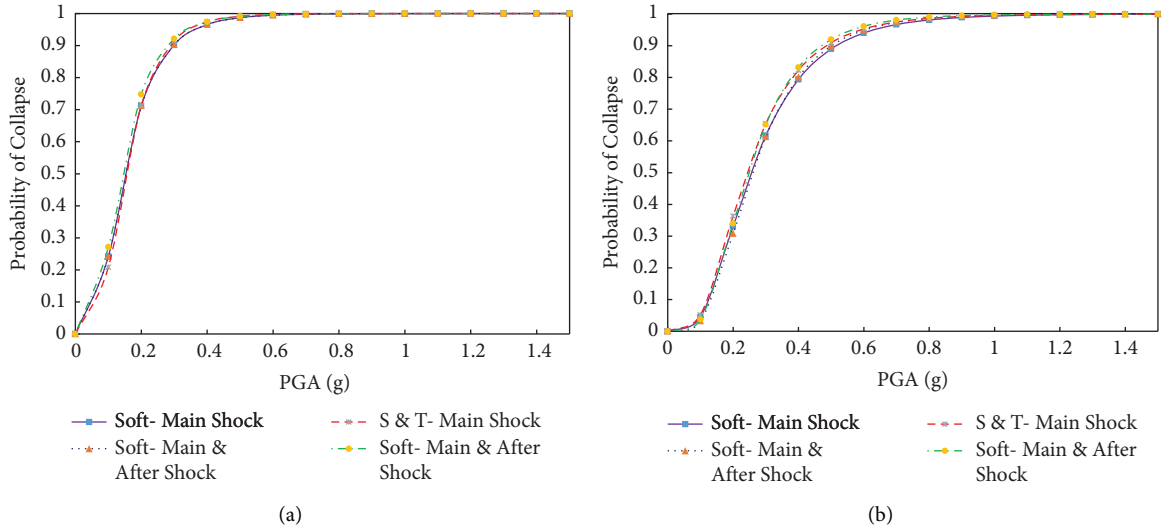

Figure 21: Continued.

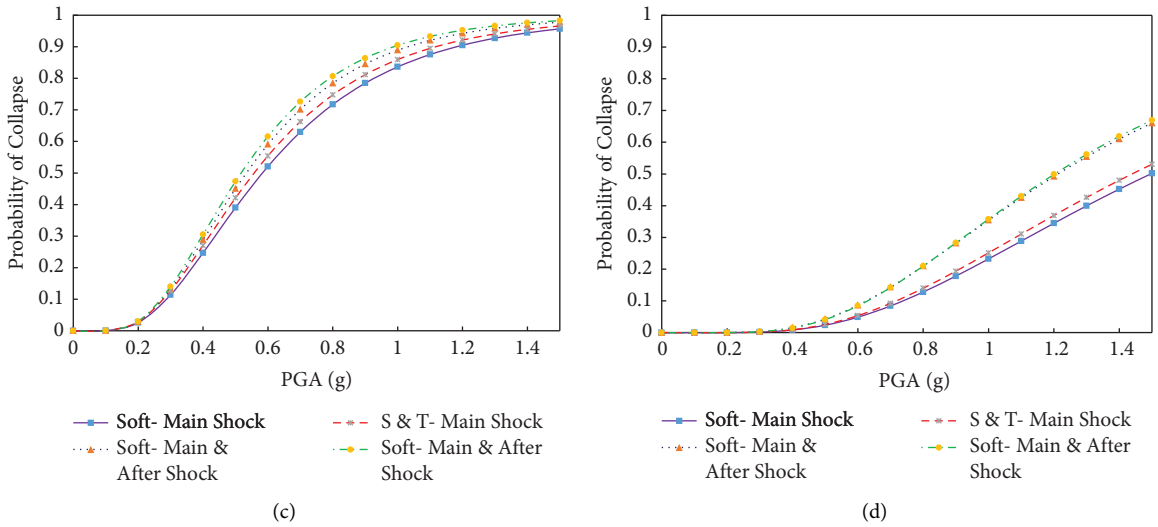

FIGURE 21: Fragility curve of a five-story structure for (a) slight damage level; (b) moderate damage level; (c) extensive damage level; and (d) complete damage level.

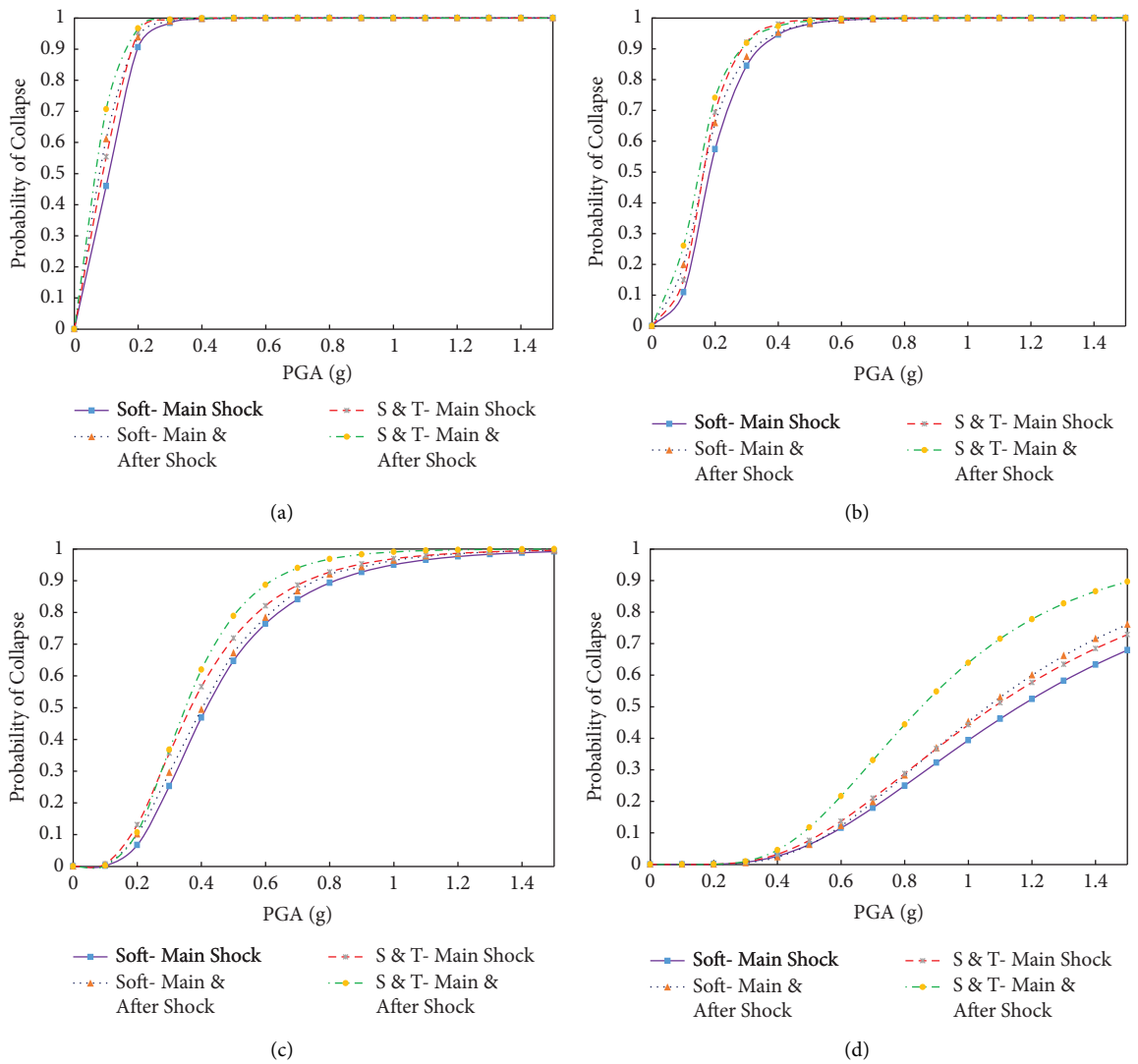

FIGURE 22: Fragility curve of a eight-story structure for (a) slight damage level; (b) moderate damage level; (c) extensive damage level; and (d) complete damage level.

these structures in the slight, moderate, extensive, and complete damage levels, respectively. In the mid-rise structure, the aftershock caused the increase rates of 12, 8.5, and 17% in the moderate, extensive, and complete damage levels, respectively. Furthermore, the aftershock causes a 5 and 9% increase in the extensive and complete damage levels of high-rise structures, respectively.

After the height difference in structures with soft-story irregularity and aftershock was examined, the torsion effect on the existing structures was analyzed. The results can be summarized as follows.

Torsion in low-rise structures with low stories had no significant effect on all four damage levels. On the other hand, with increasing height and number of stories, this effect is increased on all damage levels and is significant in high-rise ones. The numerical results obtained via examining the fragility curves and plotting the median fragility value are as follows.

The torsion in the low-rise structures did not affect all four damage levels. The damage level diagrams in the case of torsional irregularity are perfectly consistent with the regular structure in the plan. The torsion effect on the damage levels is enhanced with increasing height. Thus, in the eight-story structure, it increases the damage at four levels of slight, moderate, extensive, and complete by 15, 12, 10, and 9%, respectively.

4. Conclusion

The present study probabilistically evaluated the seismic performance of steel buildings with torsional irregularities in plan and soft story under mainshock-aftershock sequence on damage levels of buildings. The seismic sequence and simultaneous effects of the torsional irregularities on plan and soft story using the fragility curve were analyzed. The following results were obtained using the IDA method and the fragility curves in terms of the earthquake intensity and structure response.

The key findings of the analytical probabilistic seismic evaluation are as follows:

(i) An important conclusion is that the aftershock sequence followed by plan and height irregularity should not be neglected and may lead to overestimated structure capacity.

(ii) Comparing the fragility curves associated with the three-, five-, and eight-story models affected by the main earthquake shows that the effect of soft story on the damage levels is greater for low-rise structures. In general, the damage caused by the previous events and the structure irregularity significantly influence the inter-story drift related to the structural collapse.

(iii) The probability of structural collapse in a given IDR for a damaged state can be better examined by the mainshock-aftershock sequence, which is not the case in the mainshock sequence solely.

(iv) The influence of torsional irregularity is negligible on the damage levels of low-rise structures, and with the increasing number of stories, this effect increases.

(v) Comparing the effect of torsional and soft-story irregularities on the base shear rates shows that the displacement amount in the equal base shear increases by 7, 9, and 11% in three-, five-, and eight-story structures with torsional irregularity, respectively.

(vi) The findings indicate that the aftershock is more effective in low-rise structures, and aftershock impacts on the damage levels decrease with the increasing number of stories and height.

Due to the limitations in selecting a proper number of models in this paper, future research should perform additional analysis with a larger number of models to yield complete results. However, further research could examine the damage of past earthquakes and other irregularities in the international regulations, such as weak story and detachment of lateral force-resisting systems, which can also cause damage following an earthquake. The soft-story irregularity might be due to several factors, such as height increases, improper use of masonry infills, detachment and removal of gravity, and vertical load-resisting elements. It should also be noted that due to the high volume of calculations, the effects of vertical earthquake components were not considered in the analysis.

Data Availability

The data used to support the findings of this study are available from the corresponding author upon request.

Disclosure

This research is for academic and educational research, and there is no commercial discussion of the research. This paper is not currently being considered for publication elsewhere.

Conflicts of Interest

The authors declare that they have no conflicts of interest.

Acknowledgments

The authors sincerely thank all the sponsors of this research program for their support. The High-Performance Computing Center (HPCC) employees of the Shahrood University of Technology are also appreciated for their assistance in performing the nonlinear time history and incremental dynamic analyses.

References

[1] A. Belleri, E. Brunesi, R. Nascimbene, M. Pagani, and P. Riva, "Seismic performance of precast industrial facilities following major earthquakes in the Italian territory," *Journal of Performance of Constructed Facilities*, vol. 29, no. 5, Article ID 04014135, 2015.

[2] C.-H. Zhai, W. P. Wen, Z. Chen, S. Li, and L. L. Xie, "Damage spectra for the mainshock–aftershock sequence-type ground motions," *Soil Dynamics and Earthquake Engineering*, vol. 45, pp. 1–12, 2013.

[3] Y. Li, R. Song, and J. W. Van De Lindt, "Collapse fragility of steel structures subjected to earthquake mainshock-aftershock sequences," *Journal of Structural Engineering*, vol. 140, no. 12, Article ID 04014095, 2014.

[4] E. Afsar Dizaj, M. R. Salami, and M. M. Kashani, "Seismic vulnerability assessment of ageing reinforced concrete structures under real mainshock-aftershock ground motions," *Structure and Infrastructure Engineering*, vol. 18, no. 12, pp. 1674–1690, 2021.

[5] R. P. Kennedy, C. Cornell, R. Campbell, S. Kaplan, and H. Perla, "Probabilistic seismic safety study of an existing nuclear power plant," *Nuclear Engineering and Design*, vol. 59, no. 2, pp. 315–338, 1980.

[6] M. H. Razmkhah, H. Kouhestanian, and J. Shafaei, "Probabilistic seismic assessment of moment resisting steel buildings considering soft-story and torsional irregularities," *International Journal of Engineering*, vol. 34, no. 11, pp. 2476–2493, 2021.

[7] M. Reza Salami, E. Afsar Dizaj, and M. Mehdi Kashani, "The behavior of rectangular and circular reinforced concrete columns under biaxial multiple excitation," *Computer Modeling in Engineering and Sciences*, vol. 120, no. 3, pp. 677–691, 2019.

[8] R. Song, Y. Li, and J. W. Van de Lindt, "Loss estimation of steel buildings to earthquake mainshock–aftershock sequences," *Structural Safety*, vol. 61, pp. 1–11, 2016.

[9] B. Silwal and O. E. Ozbulut, "Aftershock fragility assessment of steel moment frames with self-centering dampers," *Engineering Structures*, vol. 168, pp. 12–22, 2018.

[10] Y. Pang and L. Wu, "Seismic fragility analysis of multispan reinforced concrete bridges using mainshock-aftershock sequences," *Mathematical Problems in Engineering*, vol. 2018, Article ID 1537301, 12 pages, 2018.

[11] S. Veismoradi, A. Cheraghi, and E. Darvishan, "Probabilistic mainshock-aftershock collapse risk assessment of buckling restrained braced frames," *Soil Dynamics and Earthquake Engineering*, vol. 115, pp. 205–216, 2018.

[12] F. Fattahi and S. Gholizadeh, "Seismic fragility assessment of optimally designed steel moment frames," *Engineering Structures*, vol. 179, pp. 37–51, 2019.

[13] Y. Zhang and H. V. Burton, "Pattern recognition approach to assess the residual structural capacity of damaged tall buildings," *Structural Safety*, vol. 78, pp. 12–22, 2019.

[14] F. N. Methodology and M. H.-M. R. Hazus, *Advanced Engineering Building Module: Technical and User's Manual*, FEMA Mitigation Division Washington, DC, Washington DC, USA, 2003.

[15] Road Housing and Urban Development Research Center, *Standard 2800 Iranian Code of Practice for Seismic Resistant Design of Buildings*, Road, Housing and Urban Development Research Center, Tehran, Iran, 2014.

[16] D. G. Lignos, H. Krawinkler, and A. S. Whittaker, "Prediction and validation of sidesway collapse of two scale models of a 4-story steel moment frame," *Earthquake Engineering & Structural Dynamics*, vol. 40, no. 7, pp. 807–825, 2011.

[17] I. B. C. International, *Building Code*, IBC Falls Church, Church, Virginia, USA, 2003.

[18] ASCE, *Minimum Design Loads for Buildings and Other Structures*, American Society of Civil Engineers, Reston, Virginia, USA, 2013.

[19] First Print, *Manual, Steel Construction American institute of Steel Construction*, One East Wacker Drive, Chicago, IL, USA, 2005.

[20] J. B. Mander, M. J. Priestley, and R. Park, "Theoretical stress-strain model for confined concrete," *Journal of Structural Engineering*, vol. 114, no. 8, pp. 1804–1826, 1988.

[21] M. Raghunandan, "Aftershock fragility curves and tagging assessments for a mainshock-damaged building," in *Proceedings of the 15th World Conference on Earthquake Engineering*, Lisbon, Portugal, 2012.

[22] M. Banazadeh and S. A. Jalali, "Probabilistic seismic demand assessment of steel moment frames with sideplate connections," *Amirkabir Journal of Civil Engineering*, vol. 44, no. 2, pp. 47–64, 2013.

[23] F. McKenna and G. Fenves, "The OpenSees Command Language Manual: version 1.2," *Pacific Earthquake Engineering Center*, University of California, 2001.